

# UV Volumes for Real-time Rendering of Editable Free-view Human Performance

YUE CHEN, Xi'an Jiaotong University, China

XUAN WANG, Tencent AI Lab, China

XINGYU CHEN, Xi'an Jiaotong University, China

QI ZHANG, Tencent AI Lab, China

XIAOYU LI, Tencent AI Lab, China

YU GUO, Xi'an Jiaotong University, China

JUE WANG, Tencent AI Lab, China

FEI WANG, Xi'an Jiaotong University, China

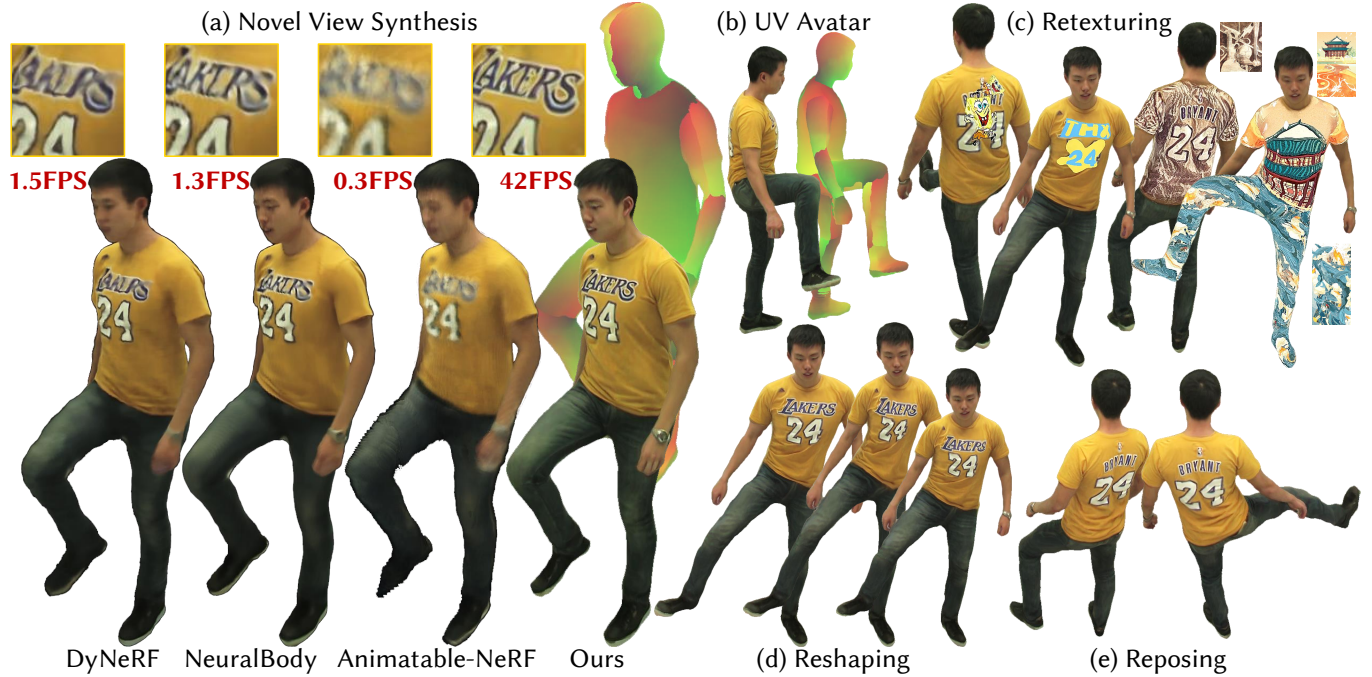


Fig. 1. We decompose the dynamic human into 3D UV Volumes and a 2D texture. The disentanglement of appearance from geometry enables us to achieve (a) real-time novel view synthesis with (b) the UV avatar, (c) retexturing of 3D human by editing the 2D texture, (d) reshaping and (e) reposing by changing the parameters of human model while keeping the texture untouched.

Neural volume rendering enables photo-realistic renderings of a human performer in free-view, a critical task in immersive VR/AR applications. But the practice is severely limited by high computational costs in the rendering process. To solve this problem, we propose the *UV Volumes*, a new approach that can render an editable free-view video of a human performer in real-time. It separates the high-frequency (i.e., non-smooth) human appearance from the 3D volume, and encodes them into 2D neural texture stacks (NTS).

Permission to make digital or hard copies of all or part of this work for personal or classroom use is granted without fee provided that copies are not made or distributed for profit or commercial advantage and that copies bear this notice and the full citation on the first page. Copyrights for components of this work owned by others than ACM must be honored. Abstracting with credit is permitted. To copy otherwise, or republish, to post on servers or to redistribute to lists, requires prior specific permission and/or a fee. Request permissions from [permissions@acm.org](mailto:permissions@acm.org).

*SIGGRAPH Conference Proceedings, Dec 2022, Daegu*

© 2022 Association for Computing Machinery.

ACM ISBN 978-1-4503-1234-5/22/07...\$15.00

<https://doi.org/10.1145/8888888.7777777>

The smooth UV volumes allow much smaller and shallower neural networks to obtain densities and texture coordinates in 3D while capturing detailed appearance in 2D NTS. For editability, the mapping between the parameterized human model and the smooth texture coordinates allows us a better generalization on novel poses and shapes. Furthermore, the use of NTS enables interesting applications, e.g., retexturing. Extensive experiments on CMU Panoptic, ZJU Mocap, and H36M datasets show that our model can render  $960 \times 540$  images in 30FPS on average with comparable photo-realism to state-of-the-art methods. The project and supplementary materials are available at <https://github.com/fanegg/UV-Volumes>.

CCS Concepts: • **Computing methodologies** → **Rendering**.

**ACM Reference Format:**

Yue Chen, Xuan Wang, Xingyu Chen, Qi Zhang, Xiaoyu Li, Yu Guo, Jue Wang, and Fei Wang. 2022. UV Volumes for Real-time Rendering of Editable Free-view Human Performance. In *Proceedings of SIGGRAPH Conference Proceedings*. ACM, New York, NY, USA, 8 pages. <https://doi.org/10.1145/8888888.7777777>

## 1 INTRODUCTION

Synthesizing free-view videos of a human performer in motion is a long-standing problem in computer graphics. Early approaches [Collet et al. 2015a] rely on obtaining an accurate 3D mesh sequence through multi-view stereo. However, the computed 3D mesh often fails to depict the complex geometry structure, resulting in limited photorealism. Methods (e.g., NeRF [Mildenhall et al. 2020]) that make use of volumetric representation and differentiable ray casting have shown promising results for novel view synthesis. These techniques have been further extended to tackle dynamic scenes.

Nonetheless, NeRF and its variants require a large number of queries against a deep Multi-Layer Perceptron (MLP). Such time-consuming computation prevents them from being applied to applications that require high rendering efficiency. In the case of static NeRF, a few methods [Garbin et al. 2021; Reiser et al. 2021; Yu et al. 2021b] have already achieved real-time performance. However, for dynamic NeRF, solutions for real-time rendering of volumetric free-view video are still lacking.

In this work, we present *UV Volumes*, a novel framework that can produce editable free-view videos of a human performer in motion and render it in real-time. Specifically, we take advantage of a pre-defined UV-unwrapping (e.g., SMPL or DensePose) of the human body to tackle the geometry (with texture coordinates) and textures in two branches. We employ a sparse 3D Convolutional Neural Networks (CNN) to transform the voxelized and structured latent codes anchored with a posed SMPL model to a 3D feature volume, in which only smooth and view-independent densities and UV coordinates are encoded. For rendering efficiency, we use a shallow MLP to decode the density and integrate the feature into the image plane by volume rendering. Each feature in the image plane is then converted to the UV coordinates individually. Accordingly, we utilize the yielded UV coordinates to query the RGB value from a pose-dependent neural texture stack (NTS). This process greatly reduces the number of queries against MLPs and enables real-time rendering.

It is worth noting that the network modules in the proposed framework only need to approximate relatively "smooth" functions. As shown in Figure 2, the magnitude spectrum of the RGB image and the corresponding UV image indicates that UV is much smoother than RGB. That is, we only model the low-frequency density and UV coordinate in the 3D volumes, and then detail the appearance in the 2D NTS, which is also spatially aligned across different poses. This feature also increases the generalization power of such modules and supports various editing operations.

We perform extensive experiments on three widely-used datasets: CMU Panoptic, ZJU Moca, and H36M datasets. The results show that the proposed approach can effectively generate editable free-view video from both dense and sparse views. The produced free-view video can be rendered in real-time with comparable photorealism to the state-of-the-art methods that have much higher computational costs. In summary, our major contributions are:

- A novel system for rendering editable human performance video in free-view and real-time.
- UV Volumes, a method that can accelerate the rendering process while preserving the high-frequency details.

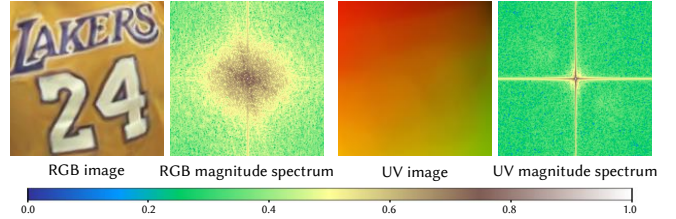


Fig. 2. Discrete Fourier Transform (DFT) for RGB and UV image. In the magnitude spectrum, the distance from each point to the midpoint describes the frequency, the direction from each point to the midpoint describes the direction of the plane wave, and the value of the point describes its amplitude. The distribution of the UV magnitude spectrum is more concentrated in the center, which indicates that the frequency of the UV image is lower.

- Extended editing applications enabled by this framework, such as reposing, retexturing, and reshaping.

## 2 RELATED WORK

**Novel View Synthesis for Static Scenes.** Novel view synthesis for static scenes is a well-explored problem. Early image-based rendering approaches [Davis et al. 2012; Gortler et al. 1996; Levoy and Hanrahan 1996] utilize densely sampled images to obtain novel views with light fields instead of explicit or accurate geometry estimation. The learning-based methods [Flynn et al. 2019; Kalantari et al. 2016; Mildenhall et al. 2019; Srinivasan et al. 2019] apply neural networks to reuse input pixels from observed viewpoints. In recent years, dramatic improvements have been achieved by neural volume rendering techniques. For instance, NeRF [Mildenhall et al. 2020] represents a static scene using a deep MLP, mapping 3D spatial locations and 2D viewing directions to volumetric density and radiance. However, rendering high-resolution scenes via NeRF is time-consuming since it requires millions of queries to obtain the density and radiance. Subsequent works [Garbin et al. 2021; Reiser et al. 2021; Yu et al. 2021a,b] attempt to accelerate the inference of vanilla NeRF in various ways, some of which achieve the real-time rendering performance, but only for static scenes.

**Free-View Video Synthesis.** Early methods [Collet et al. 2015b; Mustafa et al. 2016] rely on accurate 3D reconstruction and texture rendering captured by dome-based multi-camera systems to synthesize novel views of a dynamic scene. Recently, various neural representations have been employed in differentiable rendering to depict dynamic scenes, such as the voxels [Lombardi et al. 2019], point clouds [Wu et al. 2020], textured meshes [Thies et al. 2019], and implicit functions [Li et al. 2021b; Liu et al. 2020; Park et al. 2021a,b; Pumarola et al. 2021]. Particularly, DyNeRF [Li et al. 2021b] directly takes the latent code as the condition for time-varying scenes. Other deformation-based NeRF variants [Li et al. 2021a; Park et al. 2021a,b; Pumarola et al. 2021; Treitsch et al. 2021] take as input the monocular video, as a result, they fail to synthesize the free-view spatio-temporal visual effects. Besides, they also suffer from the high computational cost in inference and the lack of editing abilities. Geometric constraints are exploited in methods [Shao et al. 2021; Yu et al. 2021c], and a hybrid scene representation is used for efficiency in a very recent approach [Lombardi et al. 2021], but non-editable models still.

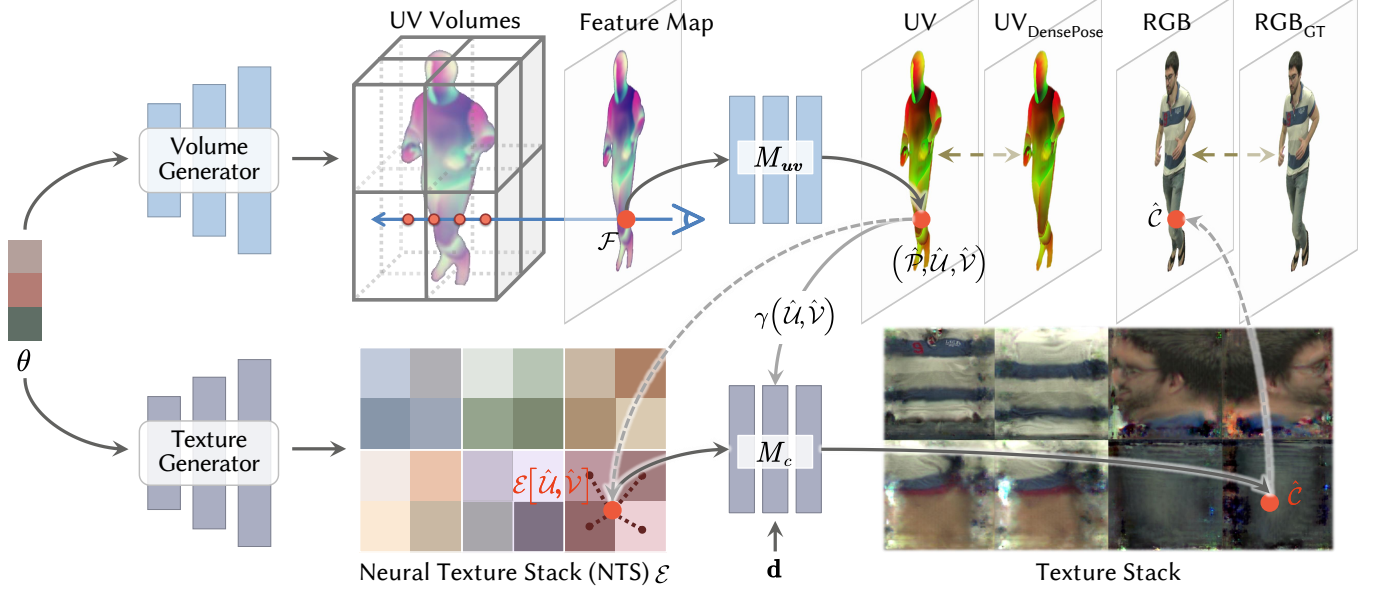


Fig. 3. Overall pipeline of proposed framework. Our model has two main branches: 1) Based on a human pose  $\theta$ , a volume generator constructs UV volumes involving the feature of UV information. Then a feature map can be rendered via differentiable raymarching and decoded to texture coordinates (UV) pixel-by-pixel. 2) A texture generator produces a pose-dependent Neural Texture Stack (NTS)  $\mathcal{E}$  encoding the highly-detailed appearance information. The UV coordinates and the texture embedding interpolated by it are passed into an MLP to predict a color  $\hat{C}$  at the desired ray direction  $d$ .

**Editable Free-View Videos.** There exist previous works that focus on the problem of producing editable free-view video or animatable avatars. ST-NeRF [Zhang et al. 2021] exploits the layered neural representation in order to move, rotate and resize individual objects in free-view videos. Methods [Peng et al. 2021a; Weng et al. 2022; Xu et al. 2021] decompose a dynamic human into a canonical neural radiance field and a skeleton-driven warp field that backward map observation-space points to canonical space. However, learning a backward warp field is highly under-constrained, since the backward warp field is pose-dependent [Chen et al. 2021]. Neural Actor [Liu et al. 2021] takes the texture map as latent variables. Unfortunately, the ground-truth texture map usually can not be obtained without high-fidelity 3D reconstruction. In contrast, without using any high-fidelity 3D reconstructions, our approach can produce editable (including reposing, reshaping and retexturing) free-view videos in real-time from both dense and sparse views.

### 3 METHOD

Given multi-view videos of a performer, our model generates an editable free-view video that supports real-time rendering. We use the availability of an off-the-shelf SMPL model and the pre-defined UV unwrap in Densepose [Güler et al. 2018] to introduce proper priors into our framework. In this section, we describe the details of our framework, which is shown in Figure 3. The two main branches in our framework are presented in turn. One is to generate the UV volumes (Sec. 3.1), and the other is the generation of NTS (Sec. 3.2). Then we provide a more detailed description of the training process in Sec. 3.3.

#### 3.1 UV Volumes

Neural radiance fields [Mildenhall et al. 2020] have been proven to produce free-viewpoint images with view consistency and high

fidelity. Nonetheless, capturing the high-fidelity appearance in a dynamic scene is time-consuming and difficult. To this end, we propose the UV volumes in which only the density and texture coordinate (i.e., UV coordinate) are encoded instead of human appearance. Given the UV image rendered by ray casting, we can use the UV coordinate to query the corresponding RGB values from the 2D NTS by employing the UV unwrap defined in Densepose.

We utilize the volume generator to construct UV volumes. First, the time-invariant latent codes anchored to a posed SMPL model are voxelized and taken as the input. Then we use the 3D sparse CNN to encode the voxelized latent codes to a 3D feature volume named the UV volumes, which contains UV information.

Given a sample image  $\mathcal{I}$  of multi-view videos, we provide a posed SMPL parameterized by human pose  $\theta$  and a set of latent codes  $z$  anchored on its vertices and then query the feature vector  $f(x, z, \theta)$  at point  $x$  from the generated UV volumes. The feature vector is fed into a shallow MLP  $M_\sigma$  to predict the volume density:

$$\sigma(x) = M_\sigma(f(x, z, \theta)). \quad (1)$$

We then apply the volume rendering [Kajiya and Von Herzen 1984] technique to render the UV feature volume into a 2D feature map. We sample  $N_i$  points  $\{x_i\}_{i=1}^{N_i}$  along the camera ray  $r$  between near and far bounds based on the posed SMPL model in 3D space. The feature at the pixel can be calculated as:

$$\mathcal{F}(r) = \sum_{i=1}^{N_i} T_i (1 - \exp(-\sigma(x_i) \delta_i)) f(x_i, z, \theta), \quad (2)$$

$$\text{where } T_i = \exp\left(-\sum_{j=1}^{i-1} \sigma(x_j) \delta_j\right),$$

where  $\delta_i = \|x_{i+1} - x_i\|_2$  is the distance between adjacent sampled points. An MLP  $M_{uv}$  is used to individually decode all the pixels





Fig. 4. The novel view synthesis results of our model on different dynamic humans.

in the yielded view-invariant feature image to their corresponding texture coordinates to generate the UV image. In specific, the texture coordinates can be represented as:

$$(\hat{\mathcal{P}}(\mathbf{r}), \hat{\mathcal{U}}(\mathbf{r}), \hat{\mathcal{V}}(\mathbf{r})) = M_{uv}(\mathcal{F}(\mathbf{r})), \quad (3)$$

where  $\hat{\mathcal{P}}$  and  $\hat{\mathcal{U}}, \hat{\mathcal{V}}$  respectively are the corresponding part assignments and UV coordinates.

### 3.2 Neural Texture Stack

Given the generated UV image, we employ the continuous texture stack encoded in the implicit neural representation to recover the color image. To extract the local relation of neural texture stack with respect to the human pose, we use a CNN texture generator  $G$  to produce the pose-dependent NTS:

$$\mathcal{E}_k = G(\theta, \mathbf{k}), \quad (4)$$

where we subdivide the body surface into  $N_k = 24$  parts, and  $\mathbf{k}$  is a one-hot label vector representing the  $k$ -th body part. At a foreground pixel, the part assignments  $\hat{\mathcal{P}}$  predicted from UV volumes (referred in Equation (3)) can be interpreted as the probability of the pixel belonging to the  $k$ -th body part, which is defined as  $\sum_{k=1}^{N_k} \hat{\mathcal{P}}_k(\mathbf{r}) = 1$ . For each human body part  $k$ , the texture generator generates corresponding neural texture stack  $\mathcal{E}_k$ . We forward propagate the generator network  $G$  once to predict all the 24 neural textures with a batch size of 24. Let  $\hat{\mathcal{U}}_k$  and  $\hat{\mathcal{V}}_k$  denote the predicted UV coordinates of the  $k$ -th body part. We sample the texture embeddings at non-integer locations  $(\hat{\mathcal{U}}_k(\mathbf{r}), \hat{\mathcal{V}}_k(\mathbf{r}))$  in a piecewise-differentiable manner using bilinear interpolation [Jaderberg et al. 2015]:

$$\mathbf{e}_k(\mathbf{r}) = \mathcal{E}_k[\hat{\mathcal{U}}_k(\mathbf{r}), \hat{\mathcal{V}}_k(\mathbf{r})]. \quad (5)$$

To model high-frequency color of human performances, we apply the positional encoding  $\gamma(\cdot)$  [Rahaman et al. 2019] to UV coordinates and viewing direction, and pass the encoded UV map with the sampled texture embedding into an MLP  $M_c$  to decode the view-dependent color  $\hat{\mathcal{C}}_k(\mathbf{r})$  of camera ray  $\mathbf{r}$  at the desired viewing direction  $\mathbf{d}$ :

$$\hat{\mathcal{C}}_k(\mathbf{r}) = M_c(\gamma(\hat{\mathcal{U}}_k(\mathbf{r}), \hat{\mathcal{V}}_k(\mathbf{r})), \mathbf{e}_k(\mathbf{r}), \mathbf{k}, \gamma(\mathbf{d})). \quad (6)$$

Following that, the color  $\hat{\mathcal{C}}(\mathbf{r})$  at each pixel is reconstructed via a weighted combination of decoded colors at  $N_k$  body parts, where

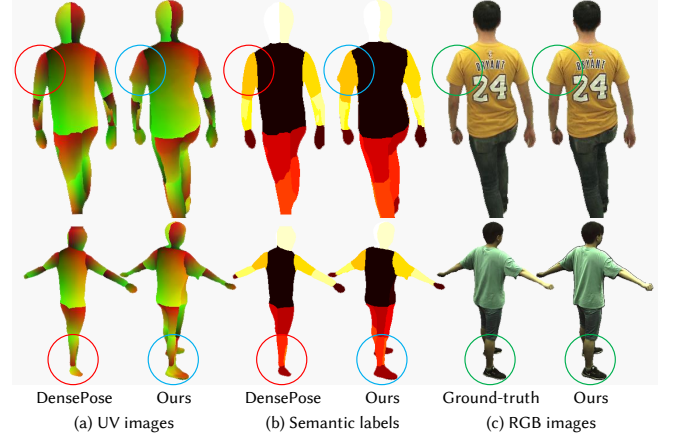


Fig. 5. Given noisy UV and semantic labels (e.g., the red circles), we can reconstruct correct UV volumes (e.g., the blue circles) under the intrinsic multi-view constraint of RGB loss (e.g., the green circles).

the weights are prescribed by part assignments  $\hat{\mathcal{P}}_k$ :

$$\hat{\mathcal{C}}(\mathbf{r}) = \sum_{k=1}^{N_k} \hat{\mathcal{P}}_k(\mathbf{r}) \hat{\mathcal{C}}_k(\mathbf{r}). \quad (7)$$

### 3.3 Training

Collecting the results of all rays  $\{\hat{\mathcal{C}}(\mathbf{r})\}^{H \times W}$ , we denote the full rendered image as  $\hat{\mathcal{I}} \in \mathbb{R}^{H \times W \times 3}$ . To learn the parameters of our model, we optimize the L2 loss between the rendered  $\hat{\mathcal{I}}$  and observed images  $\mathcal{I}$ :

$$\mathcal{L}_{\text{rgb}} = \|\hat{\mathcal{I}} - \mathcal{I}\|_2^2. \quad (8)$$

In contrast to [Mildenhall et al. 2020; Peng et al. 2021b], we can render an entire image requiring a single pass through our model. Thus, we also compare the rendered images against the ground-truth using perceptual loss [Gatys et al. 2016; Johnson et al. 2016; Ulyanov et al. 2016], which extracts feature maps by pretrained fixed VGG network  $\psi(\cdot)$  [Simonyan and Zisserman 2014] from both images and minimizes the L1-norm between them:

$$\mathcal{L}_{\text{vgg}} = \|\psi(\hat{\mathcal{I}}) - \psi(\mathcal{I})\|_1. \quad (9)$$

Datasets		PSNR $\uparrow$					SSIM $\uparrow$					LPIPS $\downarrow$					FPS $\uparrow$			
		DN	NB	AN	w/o $\mathcal{L}_p$	Ours	DN	NB	AN	w/o $\mathcal{L}_p$	Ours	DN	NB	AN	w/o $\mathcal{L}_p$	Ours	DN	NB	AN	Ours
CMU (960 $\times$ 540)	p1	30.04	29.78	27.12	30.09	<b>30.38</b>	0.968	0.962	0.936	0.963	0.966	0.088	0.099	0.135	0.055	<b>0.036</b>	1.01	0.76	0.21	<b>44.76</b>
	p2	25.56	25.68	26.13	28.51	28.78	0.939	0.942	0.903	0.952	<b>0.953</b>	0.137	0.139	0.204	0.062	<b>0.044</b>	1.45	1.28	0.34	<b>37.30</b>
	p3	27.04	27.12	24.20	29.36	<b>29.38</b>	0.955	0.956	0.874	<b>0.962</b>	<b>0.962</b>	0.154	0.142	0.259	0.062	<b>0.047</b>	2.12	1.28	0.33	<b>34.60</b>
ZJU (512 $\times$ 512)	313	<b>29.67</b>	28.82	27.50	28.44	29.11	<b>0.958</b>	0.952	0.939	0.956	<b>0.958</b>	0.084	0.088	0.124	0.068	<b>0.053</b>	2.07	1.51	0.62	<b>51.39</b>
	377	27.13	<b>28.12</b>	25.71	26.18	26.28	0.933	<b>0.949</b>	0.923	0.931	0.930	0.112	0.088	0.152	0.094	<b>0.085</b>	2.41	2.02	0.76	<b>38.70</b>
	386	<b>30.29</b>	30.12	28.51	28.38	28.48	0.938	<b>0.939</b>	0.915	0.919	0.916	0.122	0.112	0.163	0.103	<b>0.078</b>	3.00	4.89	0.91	<b>35.88</b>
H36M (500 $\times$ 500)	s9p	21.53	25.11	26.08	26.03	<b>26.19</b>	0.824	0.912	0.917	0.915	<b>0.916</b>	0.242	0.136	0.139	0.085	<b>0.084</b>	1.06	2.19	0.30	<b>40.00</b>
	s11p	21.27	24.39	25.21	25.20	25.82	0.828	0.899	0.906	0.905	<b>0.911</b>	0.313	0.193	0.174	0.118	<b>0.111</b>	1.18	1.02	0.67	<b>33.41</b>
	s1p	18.91	23.24	23.43	23.83	<b>23.98</b>	0.781	0.909	0.901	<b>0.911</b>	<b>0.911</b>	0.332	0.149	0.162	0.094	<b>0.093</b>	1.38	0.97	0.50	<b>41.43</b>

Table 1. Quantitative results of novel view synthesis. We achieve competitive PSNR and SSIM while outperforming the others on LPIPS and FPS.

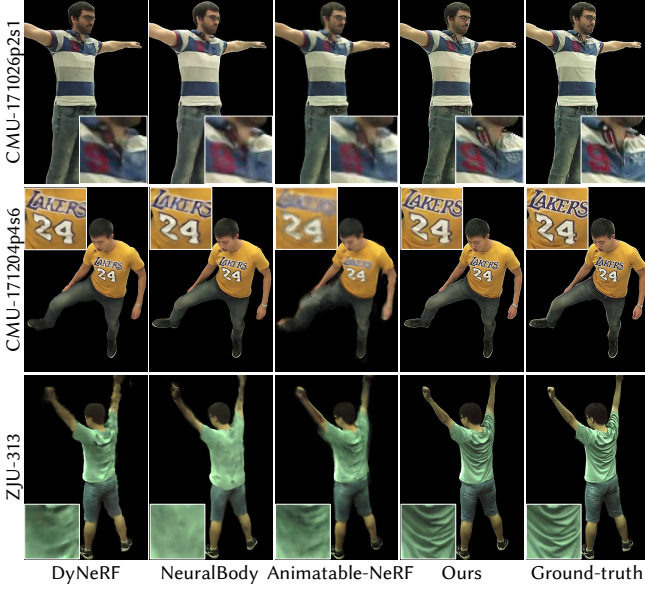


Fig. 6. Qualitative results of novel view synthesis on CMU Panoptic, ZJU Mocap. It is illustrated that our method produces the high-fidelity novel synthesis results. All the baseline methods suffer from blurry textures, especially letters and wrinkles.

To warm-start the UV volumes and regularize its solution space, we leverage the pre-trained DensePose model. In particular, we perform the DensePose on the training data to produce the DensePose UV image as pseudo supervision, to regularize the UV volumes under semantic loss  $\mathcal{L}_p$  and UV-metric loss  $\mathcal{L}_{uv}$  between the DensePose outputs and our UV predictions:

$$\mathcal{L}_p = \sum_{k=1}^{N_k} \mathcal{P}_k \log(\hat{\mathcal{P}}_k),$$

$$\mathcal{L}_{uv} = \sum_{k=1}^{N_k} \mathcal{P}_k \left( \left\| \hat{\mathcal{U}}_k - \mathcal{U}_k \right\|_2^2 + \left\| \hat{\mathcal{V}}_k - \mathcal{V}_k \right\|_2^2 \right), \quad (10)$$

where  $N_k$  is the number of body parts, and  $\mathcal{P}_k$  and  $\hat{\mathcal{P}}_k$  are respectively the multi-class semantic probability at the  $k$ -th part of DensePose outputs and UV volumes predictions. Similarly,  $\mathcal{U}_k, \mathcal{V}_k$  and  $\hat{\mathcal{U}}_k, \hat{\mathcal{V}}_k$  are the DensePose and UV volumes predicted UV coordinates at the  $k$ -th part.  $\mathcal{L}_p$  is chosen as a multi-class cross-entropy loss to encourage rendered part labels to be consistent with provided DensePose labels, and  $\mathcal{L}_{uv}$  promotes to generate inter-frame consistent UV coordinates.

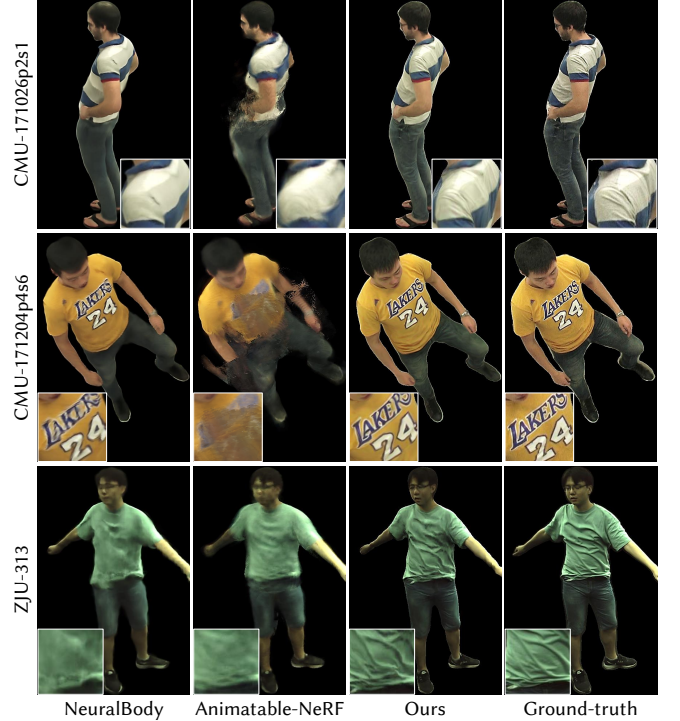


Fig. 7. Qualitative results of novel pose generalization on CMU Panoptic, ZJU Mocap. Benefiting from the UV volumes and NTS that give our models better generalization ability, our method performs better on novel poses, especially for preserving sharp image details.

We present the UV images predicted by our UV volumes and the pseudo supervision of DensePose in Figure 5. Given noisy semantic and UV labels (e.g., the blue circles), we can reconstruct correct UV volumes (e.g., the red circles) under the intrinsic multi-view constraint of RGB loss (e.g., the green circles). As shown in the second row of Figure 5, it can be observed that UV volumes successfully recovered the UV images even though the provided DensePose supervision is incorrect.

Given the binary human mask  $\mathcal{S}$  for the observed image  $\mathcal{I}$ , we propose a silhouette loss to facilitate UV volumes modeling a more fine-grained geometry:

$$T(r) = \exp \left( - \sum_{j=1}^{N_i-1} \sigma(x_j) \delta_j \right),$$

$$\mathcal{L}_s = \sum_{r \in \mathcal{R}} (\mathcal{S}(r)(1 - T(r)) + (1 - \mathcal{S}(r))T(r)), \quad (11)$$

Methods	CMU(960×540)			ZJU(512×512)			H36M(500×500)		
	PSNR↑	SSIM↑	LPIPS↓	PSNR↑	SSIM↑	LPIPS↓	PSNR↑	SSIM↑	LPIPS↓
NB	25.94	0.918	0.146	24.51	0.918	0.120	25.54	0.884	0.170
AN	23.65	0.883	0.208	24.55	0.911	0.153	25.00	0.873	0.170
Ours	26.20	0.927	0.073	23.69	0.910	0.104	25.04	0.874	0.141

Table 2. Quantitative results of novel pose generalization. We achieve competitive PSNR and SSIM while outperforming the others on LPIPS.

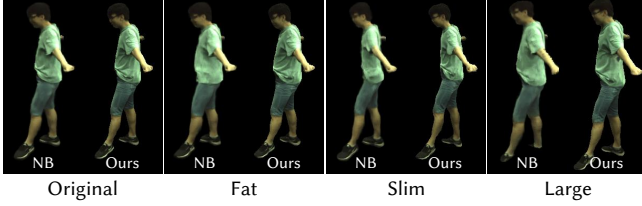


Fig. 8. Qualitative results of reshaping. By changing the SMPL parameters  $\beta$ , we can conveniently make the human performer fatter, slimmer, or larger. In each pair of results, the result of NeuralBody is shown on the left, and our result is on the right. Obviously, more details and consistency are preserved in our results in varying shapes.

where  $T(r)$  is accumulated transmittance. The value of mask  $S(r)$  in the foreground is zero, and the background is one.

We combine the aforementioned losses and jointly train our model to optimize the full objective:

$$\mathcal{L} = \mathcal{L}_{rgb} + \lambda_{vgg} \mathcal{L}_{vgg} + \lambda_p \mathcal{L}_p + \lambda_{uv} \mathcal{L}_{uv} + \lambda_s \mathcal{L}_s. \quad (12)$$

## 4 EXPERIMENTS

To demonstrate the effectiveness and efficiency of our method, we perform extensive experiments. We report quantitative results using four standard metrics: PSNR, SSIM, LPIPS, and FPS. And the qualitative experiments illustrate our method produces photo-realistic images in different tasks, e.g., novel view synthesis, reposing, reshaping, and retexturing.

**Dataset.** We perform experiments on several types of datasets which consist of calibrated and synchronized multi-view videos. We use 26 and 20 training views on CMU Panoptic dataset [Joo et al. 2017] with  $960 \times 540$  resolution and ZJU Mocap dataset [Peng et al. 2021b] with  $512 \times 512$  resolution, respectively. The most challenging one is the H36M dataset [Ionescu et al. 2013] with  $500 \times 500$  resolution, where only three cameras are available for training. The evaluation is done on the hold-out cameras (novel views) or hold-out segments of the sequence (novel poses).

**Baselines.** To validate our method, we compare it against several state-of-the-art free-view video synthesis techniques: 1) DN: DyNeRF [Li et al. 2021b], which takes time-varying latent codes as the conditions for dynamic scenes; and 2) NB: NeuralBody [Peng et al. 2021b], which takes as input the posed human model with structured time-invariant latent codes and generates a pose-conditioned neural radiance field; 3) AN: Animatable-NeRF, which uses neural blend weight fields to generate correspondences between observation and canonical space.

**Novel View Synthesis.** For comparison, we synthesize images of training poses in hold-out test views. Table 1 shows the comparison of our method against baselines, which demonstrates that our method performs best LPIPS and FPS among all methods. Specifically, we achieve rendering the free-view videos of human performances in 30FPS with the help of UV volumes. Note that LPIPS agrees



Fig. 9. Qualitative results of retexturing. The presented framework allows us to edit the texture by drawing patterns on the NTS conveniently. The rich texture patterns are well preserved and transferred to correct semantic areas in different poses, which demonstrates that UV Volumes not only successfully change the texture under the edited frame but also can be transferred to a novel one with the modeled dynamics.

surprisingly well with human visual perception, which indicates that our synthesis is more visually similar to ground-truth.

Figure 6 presents the qualitative comparison of our method with baselines. Baselines fail to preserve the sharp image details, whose rendering is blurry and even split. In contrast, our method can accurately capture the high-frequency details like letters, numbers and wrinkles on shirts and the belt on pants benefiting from our NTS model. Furthermore, we show the view synthesis results of dynamic humans in Figure 4, which indicate that our method generates high-quality appearance results even with rich textures and challenging motions. Note the rightmost example is from the H36M dataset with only 4 views. Please refer to the supplementary material and video for more results.

**Reposing.** We perform reposing on the human performer with novel motions. As DyNeRF is not designed for editing tasks, we compare our method against NeuralBody and Animatable-NeRF. As shown in Table 2, quantitative results demonstrate that our method achieves competitive PSNR and SSIM while outperforming others on LPIPS.

The qualitative results are shown in Figure 7. For novel human poses, NeuralBody gives blurry and distorted rendering results while Animatable-NeRF even produces split humans due to a highly under-constrained backward warp field from observation to canonical space. In contrast, synthesized images of our method achieve better visual quality with reasonable high-definition dynamic textures. The results indicate that using smooth UV volumes in 3D and encoding texture in 2D has better controllability on the novel pose generalization than directly modeling a pose-conditioned neural radiance field.

**Reshaping.** We demonstrate that our approach can edit the shape of reconstructed human performance by changing the shape parameters of the SMPL model. We report the qualitative results in Figure 1 and Figure 8. NeuralBody fails to infer the reasonable changes of the cloth, while our method generalizes well on novel shapes.



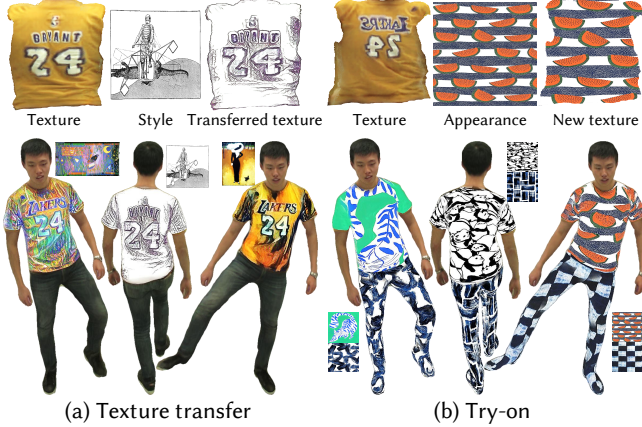


Fig. 10. Given any arbitrary artistic style or cloth appearance, we can render (a) a 3D dynamic human with the transferred texture or perform (b) a 3D virtual try-on in real-time.

	Novel View Synthesis			Novel Pose Generation		
	PSNR $\uparrow$	SSIM $\uparrow$	LPIPS $\downarrow$	PSNR $\uparrow$	SSIM $\uparrow$	LPIPS $\downarrow$
No Warm-start Loss	30.37	0.964	0.060	26.14	0.917	0.076
No Perceptual Loss	30.09	0.963	0.055	26.05	0.919	0.079
No Silhouette Loss	17.47	0.874	0.207	16.95	0.860	0.218
Complete Model	30.38	0.966	0.036	26.20	0.927	0.073

Table 3. Results of models under different training settings.

**Retexturing.** With the learned dense correspondence of UV volumes and neural texture, we can edit the 3D cloth with a user-provided 2D texture, as shown in Figure 9. Visually inspected, the rich texture patterns are well preserved and transferred to correct semantic areas in different poses. Moreover, our model supports changing textures’ style and appearance, which are presented in Figure 10. Thanks to the style transfer network [Ghiasi et al. 2017], we can perform arbitrary artistic stylizations on 3D human performance. Given any fabric texture, we can even dress the performer in various appearances, which enables 3D virtual try-on in real-time.

#### 4.1 Ablation Studies

We conduct ablation studies on performer p1 of the CMU dataset. As shown in Table 3, we analyze the effects of different losses for the proposed approach by removing warm-start loss, perceptual loss and silhouette loss, respectively. Then, we analyze the time consumption of each module. We encourage the reader to see the supplement for additional ablations, discussion of model design, and other experimental results.

**Impact of warm-start loss.** We present using semantic and UV-metric loss to warm-start the UV volumes and constrain its solution space. To prove the effectiveness of this process, we train an ablation (No Warm-start Loss) built upon our full model by eliminating the warm-start loss. It gives lower performance in all metrics, especially the LPIPS increased a lot when rendering novel views. This comparison indicates that the warm-start loss yields better information reuse of different frames by transforming the observation XYZ coordinates to canonical UV coordinates defined by the consistent semantic and UV-metric loss.

Method	Novel Pose Generation					
	Sparse CNN	Novel View Synthesis				
		Density	Color Model			Rendering
Ours	48.78	7.08	UV	NTS	RGB	1.73
			1.53	7.52	1.60	
			9.12			
		19.46				
	68.23					
NB	52.04	84.38	546.81			32.65
		663.84				
	715.88					

Table 4. Time analysis of each module in milliseconds(ms).

**Impact of perceptual loss.** Thanks to the UV volumes, we can render an entire image by a single pass during training, allowing us to use perceptual loss. Using the same model but training without the perceptual loss (No Perceptual Loss) gives a lower performance in all metrics, especially the PSNR and LPIPS. This comparison illustrates that perceptual loss can improve the visual quality of synthesized images.

**Impact of silhouette loss.** To facilitate the UV volumes modeling a more fine-grained geometry, we employ a silhouette loss by using the 2D binary mask of the human performer. We present an ablation (No Silhouette Loss) built upon our full model by eliminating the silhouette loss, as shown in Table 3. It is obvious that No Silhouette Loss gives the worst performance in all metrics among all ablations. This comparison demonstrates that our geometry does benefit from the silhouette loss, which can be seen in the supplement to get an intuitive visual experience.

#### 4.2 Time Consumption

We analyze the time consumption of each module in our framework and the corresponding module in NeuralBody [Peng et al. 2021b] on ZJU Mocap performer 313, as shown in Table 4. On average, it takes 48.78 ms for us to obtain the UV volumes from the posed human model. Then, our method takes only 19.46 ms (51FPS) to access the free-view renderings, which benefits from the smooth UV volumes that allow the much smaller and shallower to obtain densities and texture coordinates in 3D while capturing detailed appearance in 2D NTS. On the contrary, NeuralBody spends 663.84 ms (1.5FPS) to synthesize novel views, which prevents it from being used in applications that require running in real-time. Even on the novel pose generalization task, our method can reach 68.23 milliseconds per frame (14FPS) as well. All experiments are run on a single NVIDIA A100 GPU.

### 5 CONCLUSIONS

We have presented the UV volumes for free-view video synthesis of a human performer. It is the first method to generate a real-time free-view video with editing ability. The key idea is to employ the smooth UV volumes and highly-detailed textures in an implicit neural texture stack. Extensive experiments have demonstrated both the effectiveness and efficiency of our method. In addition to improving efficiency, our approach can also support editing, e.g., reposing, reshaping, or retexturing the human performer in the free-view videos.

## REFERENCES

- Xu Chen, Yufeng Zheng, Michael J Black, Otmar Hilliges, and Andreas Geiger. 2021. SNARF: Differentiable Forward Skinning for Animating Non-Rigid Neural Implicit Shapes. In *International Conference on Computer Vision (ICCV)*.
- Alvaro Collet, Ming Chuang, Pat Sweeney, Don Gillett, Dennis Evseev, David Calabrese, Hugues Hoppe, Adam Kirk, and Steve Sullivan. 2015a. High-quality streamable free-viewpoint video. *ACM Transactions on Graphics (ToG)* 34, 4 (2015), 1–13.
- Alvaro Collet, Ming Chuang, Pat Sweeney, Don Gillett, Dennis Evseev, David Calabrese, Hugues Hoppe, Adam Kirk, and Steve Sullivan. 2015b. High-quality streamable free-viewpoint video. *ACM Transactions on Graphics (ToG)* 34, 4 (2015), 1–13.
- Abe Davis, Marc Levoy, and Fredo Durand. 2012. Unstructured light fields. In *Computer Graphics Forum*, Vol. 31. Wiley Online Library, 305–314.
- John Flynn, Michael Broxton, Paul Debevec, Matthew DuVall, Graham Fyfe, Ryan Overbeck, Noah Snavely, and Richard Tucker. 2019. Deepview: View synthesis with learned gradient descent. In *Proceedings of the IEEE/CVF Conference on Computer Vision and Pattern Recognition*. 2367–2376.
- Stephan J Garbin, Marek Kowalski, Matthew Johnson, Jamie Shotton, and Julien Valentin. 2021. Fastnerf: High-fidelity neural rendering at 200fps. *arXiv preprint arXiv:2103.10380* (2021).
- Leon A Gatys, Alexander S Ecker, and Matthias Bethge. 2016. Image style transfer using convolutional neural networks. In *Proceedings of the IEEE conference on computer vision and pattern recognition*. 2414–2423.
- Golnaz Ghiasi, Honglak Lee, Manjunath Kudlur, Vincent Dumoulin, and Jonathon Shlens. 2017. Exploring the structure of a real-time, arbitrary neural artistic stylization network. *arXiv preprint arXiv:1705.06830* (2017).
- Steven J Gortler, Radek Grzeszczuk, Richard Szeliski, and Michael F Cohen. 1996. The lumigraph. In *Proceedings of the 23rd annual conference on Computer graphics and interactive techniques*. 43–54.
- Rıza Alp Güler, Natalia Neverova, and Iasonas Kokkinos. 2018. Densepose: Dense human pose estimation in the wild. In *Proceedings of the IEEE conference on computer vision and pattern recognition*. 7297–7306.
- Catalin Ionescu, Dragos Papava, Vlad Olaru, and Cristian Sminchisescu. 2013. Human3.6m: Large scale datasets and predictive methods for 3d human sensing in natural environments. *IEEE transactions on pattern analysis and machine intelligence* 36, 7 (2013), 1325–1339.
- Max Jaderberg, Karen Simonyan, Andrew Zisserman, et al. 2015. Spatial transformer networks. *Advances in neural information processing systems* 28 (2015), 2017–2025.
- Justin Johnson, Alexandre Alahi, and Li Fei-Fei. 2016. Perceptual losses for real-time style transfer and super-resolution. In *European conference on computer vision*. Springer, 694–711.
- Hanbyul Joo, Tomas Simon, Xulong Li, Hao Liu, Lei Tan, Lin Gui, Sean Banerjee, Timothy Godisart, Bart Nabbe, Iain Matthews, et al. 2017. Panoptic studio: A massively multiview system for social interaction capture. *IEEE transactions on pattern analysis and machine intelligence* 41, 1 (2017), 190–204.
- James T Kajiya and Brian P Von Herzen. 1984. Ray tracing volume densities. *ACM SIGGRAPH computer graphics* 18, 3 (1984), 165–174.
- Nima Khademi Kalantari, Ting-Chun Wang, and Ravi Ramamoorthi. 2016. Learning-based view synthesis for light field cameras. *ACM Transactions on Graphics (TOG)* 35, 6 (2016), 1–10.
- Marc Levoy and Pat Hanrahan. 1996. Light field rendering. In *Proceedings of the 23rd annual conference on Computer graphics and interactive techniques*. 31–42.
- Tianye Li, Mira Slavcheva, Michael Zollhoefer, Simon Green, Christoph Lassner, Changil Kim, Tanner Schmidt, Steven Lovegrove, Michael Goesele, and Zhaoyang Lv. 2021b. Neural 3d video synthesis. *arXiv preprint arXiv:2103.02597* (2021).
- Zhengqi Li, Simon Niklaus, Noah Snavely, and Oliver Wang. 2021a. Neural scene flow fields for space-time view synthesis of dynamic scenes. In *Proceedings of the IEEE/CVF Conference on Computer Vision and Pattern Recognition*. 6498–6508.
- Lingjie Liu, Jiatao Gu, Kyaw Zaw Lin, Tat-Seng Chua, and Christian Theobalt. 2020. Neural sparse voxel fields. *arXiv preprint arXiv:2007.11571* (2020).
- Lingjie Liu, Marc Habermann, Viktor Rudnev, Kripasindhu Sarkar, Jiatao Gu, and Christian Theobalt. 2021. Neural actor: Neural free-view synthesis of human actors with pose control. *ACM Transactions on Graphics (TOG)* 40, 6 (2021), 1–16.
- Stephen Lombardi, Tomas Simon, Jason Saragih, Gabriel Schwartz, Andreas Lehrmann, and Yaser Sheikh. 2019. Neural volumes: Learning dynamic renderable volumes from images. *arXiv preprint arXiv:1906.07751* (2019).
- Stephen Lombardi, Tomas Simon, Gabriel Schwartz, Michael Zollhoefer, Yaser Sheikh, and Jason Saragih. 2021. Mixture of volumetric primitives for efficient neural rendering. *ACM Transactions on Graphics (TOG)* 40, 4 (2021), 1–13.
- Ben Mildenhall, Pratul P Srinivasan, Rodrigo Ortiz-Cayon, Nima Khademi Kalantari, Ravi Ramamoorthi, Ren Ng, and Abhishek Kar. 2019. Local light field fusion: Practical view synthesis with prescriptive sampling guidelines. *ACM Transactions on Graphics (TOG)* 38, 4 (2019), 1–14.
- Ben Mildenhall, Pratul P Srinivasan, Matthew Tancik, Jonathan T Barron, Ravi Ramamoorthi, and Ren Ng. 2020. Nerf: Representing scenes as neural radiance fields for view synthesis. In *European conference on computer vision*. Springer, 405–421.
- Armin Mustafa, Hansung Kim, Jean-Yves Guillemaut, and Adrian Hilton. 2016. Temporally coherent 4d reconstruction of complex dynamic scenes. In *Proceedings of the IEEE Conference on Computer Vision and Pattern Recognition*. 4660–4669.
- Keunhong Park, Utkarsh Sinha, Jonathan T Barron, Sofien Bouaziz, Dan B Goldman, Steven M Seitz, and Ricardo Martin-Brualla. 2021a. Nerfies: Deformable neural radiance fields. In *Proceedings of the IEEE/CVF International Conference on Computer Vision*. 5865–5874.
- Keunhong Park, Utkarsh Sinha, Peter Hedman, Jonathan T Barron, Sofien Bouaziz, Dan B Goldman, Ricardo Martin-Brualla, and Steven M Seitz. 2021b. Hypernerf: A higher-dimensional representation for topologically varying neural radiance fields. *arXiv preprint arXiv:2106.13228* (2021).
- Sida Peng, Junting Dong, Qianqian Wang, Shangzhan Zhang, Qing Shuai, Xiaowei Zhou, and Hujun Bao. 2021a. Animatable Neural Radiance Fields for Modeling Dynamic Human Bodies. In *ICCV*.
- Sida Peng, Yuanqing Zhang, Yinghao Xu, Qianqian Wang, Qing Shuai, Hujun Bao, and Xiaowei Zhou. 2021b. Neural body: Implicit neural representations with structured latent codes for novel view synthesis of dynamic humans. In *Proceedings of the IEEE/CVF Conference on Computer Vision and Pattern Recognition*. 9054–9063.
- Albert Pumarola, Enric Corona, Gerard Pons-Moll, and Francesc Moreno-Noguer. 2021. D-nerf: Neural radiance fields for dynamic scenes. In *Proceedings of the IEEE/CVF Conference on Computer Vision and Pattern Recognition*. 10318–10327.
- Nasim Rahaman, Aristide Baratin, Devansh Arpit, Felix Draxler, Min Lin, Fred Hamprecht, Yoshua Bengio, and Aaron Courville. 2019. On the spectral bias of neural networks. In *International Conference on Machine Learning*. PMLR, 5301–5310.
- Christian Reiser, Songyou Peng, Yiyi Liao, and Andreas Geiger. 2021. KiloNeRF: Speeding up Neural Radiance Fields with Thousands of Tiny MLPs. *arXiv preprint arXiv:2103.13744* (2021).
- Ruizhi Shao, Hongwen Zhang, He Zhang, Yanpei Cao, Tao Yu, and Yebin Liu. 2021. Doublefield: Bridging the neural surface and radiance fields for high-fidelity human rendering. *arXiv preprint arXiv:2106.03798* (2021).
- Karen Simonyan and Andrew Zisserman. 2014. Very deep convolutional networks for large-scale image recognition. *arXiv preprint arXiv:1409.1556* (2014).
- Pratul P Srinivasan, Richard Tucker, Jonathan T Barron, Ravi Ramamoorthi, Ren Ng, and Noah Snavely. 2019. Pushing the boundaries of view extrapolation with multiplane images. In *Proceedings of the IEEE/CVF Conference on Computer Vision and Pattern Recognition*. 175–184.
- Justus Thies, Michael Zollhöfer, and Matthias Nießner. 2019. Deferred neural rendering: Image synthesis using neural textures. *ACM Transactions on Graphics (TOG)* 38, 4 (2019), 1–12.
- Edgar Tretschk, Ayush Tewari, Vladislav Golyanik, Michael Zollhöfer, Christoph Lassner, and Christian Theobalt. 2021. Non-rigid neural radiance fields: Reconstruction and novel view synthesis of a dynamic scene from monocular video. In *Proceedings of the IEEE/CVF International Conference on Computer Vision*. 12959–12970.
- Dmitry Ulyanov, Vadim Lebedev, Andrea Vedaldi, and Victor S Lempitsky. 2016. Texture networks: Feed-forward synthesis of textures and stylized images. In *ICML*, Vol. 1. 4.
- Chung-Yi Weng, Brian Curless, Pratul P Srinivasan, Jonathan T Barron, and Ira Kemelmacher-Shlizerman. 2022. HumanNeRF: Free-viewpoint Rendering of Moving People from Monocular Video. *arXiv preprint arXiv:2201.04127* (2022).
- Minye Wu, Yuehao Wang, Qiang Hu, and Jingyi Yu. 2020. Multi-view neural human rendering. In *Proceedings of the IEEE/CVF Conference on Computer Vision and Pattern Recognition*. 1682–1691.
- Hongyi Xu, Thiemo Alldieck, and Cristian Sminchisescu. 2021. H-nerf: Neural radiance fields for rendering and temporal reconstruction of humans in motion. *Advances in Neural Information Processing Systems* 34 (2021).
- Alex Yu, Sara Fridovich-Keil, Matthew Tancik, Qinhong Chen, Benjamin Recht, and Angjoo Kanazawa. 2021a. Plenoxels: Radiance Fields without Neural Networks. *arXiv preprint arXiv:2112.05131* (2021).
- Alex Yu, Ruilong Li, Matthew Tancik, Hao Li, Ren Ng, and Angjoo Kanazawa. 2021b. Plenotrees for real-time rendering of neural radiance fields. *arXiv preprint arXiv:2103.14024* (2021).
- Tao Yu, Zerong Zheng, Kaiwen Guo, Pengpeng Liu, Qionghai Dai, and Yebin Liu. 2021c. Function4d: Real-time human volumetric capture from very sparse consumer rgbd sensors. In *Proceedings of the IEEE/CVF Conference on Computer Vision and Pattern Recognition*. 5746–5756.
- Jiakai Zhang, Xinhang Liu, Xinyi Ye, Fuqiang Zhao, Yanshun Zhang, Minye Wu, Yingliang Zhang, Lan Xu, and Jingyi Yu. 2021. Editable free-viewpoint video using a layered neural representation. *ACM Transactions on Graphics (TOG)* 40, 4 (2021), 1–18.